DOI: 10.1002/cbic.200900031

Detection of RNA Hybridization by Pyrene-Labeled Probes

Guojie Wang,[a] Georgii V. Bobkov,[b] Sergey N. Mikhailov,[b] Guy Schepers,[c] Arthur Van Aerschot,[c] Jef Rozenski,[c] Mark Van der Auweraer,*[a] Piet Herdewijn,*[c] and Steven De Feyter*[a]

By covalently attaching pyrene chromophores with different linkers onto altritol nucleotides or ribonucleotides, and by varying the number of these pyrene modified altritol nucleotides and ribonucleotides in HNA (hexitol nucleic acid) and RNA, respectively, we have explored the general applicability of pyrene absorbance and especially fluorescence as a probe to monitor RNA hybridization. The results reveal that the backbone of the probes, the number of pyrene units attached and the nature of the tether can all substantially affect the absorbance and fluorescence properties of the probes both in single strand and double strand form. Moreover, the strength of hybridization is also affected. The disappearance of pyrene aggregate/excimer emission and simultaneous increase in monomer emission intensity of the multipyrene-labeled probes has been successfully used to monitor the hybridization of oligonucleotides, including a hairpin structure. Differences in optical response between the HNA- and RNA-skeleton probes upon hybridization indicate that the interaction of pyrene with the nucleobases in both types of duplexes is different.

Introduction

In view of the developments in the field of RNA biology, it is important to develop probes for the sequence specific detection of RNA. An easy way to do this is to use fluorescence as a detection system and to be able to discriminate between single stranded and duplex RNA. A large change in absorption or fluorescence or a wavelength shift upon hybridization of the probe covalently bond to RNA with the target RNA might be diagnostic for the presence of the complementary RNA in the solution. RNA and DNA molecular diagnostics by fluorescent labeling has indeed been a research topic of increasing interest.[1] Pyrene is widely used in this field because its fluorescence quantum efficiency is high and its fluorescence is largely affected by environmental factors, such as solvent and nearby nucleotide bases. The photophysics of pyrenes and pyrene derivatives in aqueous and other organized media have been studied in detail.[2] Fluorescent pyrene-labeled probes can be used to detect the hybridization of DNA and RNA since it is reported that their absorbance and fluorescence properties can change upon hybridization; this also depends on the structure of probes and targets. For instance, it was reported for some probes that pyrene is highly emissive in the monomer-emission region when attached to a RNA duplex but not to a DNA duplex. This was attributed to the difference in environment for the pyrene probes appended to the sugar unit of pyrene-RNA and pyrene-DNA duplexes.[3–5] Yet for some other pyrene-labeled DNA oligonucleotides (ONs), the fluorescence emission was reported to increase rather than decrease upon hybridization.[6–7]

Although pyrene has been used as a fluorescent probe to monitor the hybridization or tertiary folding of nucleic acids,[8] pyrene-oligonucleotide probes based on monomer emission intensity are usually disturbed by fluorescence quenching through an electron-migration process between excited pyrene and nucleotide bases.[9–11] The quenched fluorescence may decrease the detection ability of the probes. This means that for some DNA duplexes the fluorescence quenched by the flanking C/G base pair differs little from that of a single stranded probe.[12–13]

To overcome this disadvantage, pyrene excimer emission instead of monomer emission has been explored for monitoring RNA and DNA hybridization,[14–21] as pyrene-excimer emission is less sensitive to quenching by nucleobases than monomer emission.

Very recently pyrene excimer signaling molecular beacons for probing nucleic acids were reported.[14] In another study, a pyrene-labeled DNA probe bearing a row of five adjacent

[a] Dr. G. Wang, Prof. M. Van der Auweraer, Prof. S. De Feyter
Department of Chemistry, Division of Molecular and Nanomaterials
Laboratory of Photochemistry and Spectroscopy, and INPAC-Institute for Nanoscale Physics and Chemistry, Katholieke Universiteit Leuven
Celestijnenlaan 200 F, 3001 Leuven (Belgium)
Fax: (+32) 16 327990
E-mail: mark.vanderauweraer@chem.kuleuven.be
steven.defeyter@chem.kuleuven.be

[b] G. V. Bobkov, Prof. S. N. Mikhailov
Engelhardt Institute of Molecular Biology, Russian Academy of Sciences
Vavilov street 32, Moscow, 119991 (Russia)

[c] G. Schepers, Prof. A. Van Aerschot, Prof. J. Rozenski, Prof. P. Herdewijn
Laboratory of Medicinal Chemistry, Rega Institute
Katholieke Universiteit Leuven
Minderbroedersstraat 10, B 3000, Leuven (Belgium)
E-mail: piet.herdewijn@rega.kuleuven.be

Supporting information for this article is available on the WWW under http://dx.doi.org/10.1002/cbic.200900031: synthesis and characterization of pyrene-labeled adenine nucleosides; temperature-dependent relative absorbance for the single strands; temperature-dependent absorption spectra; temperature-dependent fluorescence spectra; melting curves; excitation spectra.

chromophores has been reported to be sensitive to the structure of DNA, as the excimer fluorescence could be enhanced 22-fold upon hybridization.[15] It has also been reported that the shift of the excimer emission band can be used as a signal to detect hybridization, as the excimer fluorescence could red-shift or blue-shift upon hybridization by the interstrand-stacked pyrenes.[16] Although both monomer and excimer emission of pyrene-labeled probes has been investigated in detail, the often complex response depends on the structure of the probe.

In this paper, we report the synthesis and hybridization of two kinds of pyrene-labeled probes with RNA targets. These pyrene-labeled probes include: 1) so-called hexitol nucleic acid (HNA)-skeleton probes, which contain one or more pyrene functionalized altritol nucleotides (adenine derivative of 3-*O*-(pyren-1-ylmethyl)-2-deoxy-D-altritol incorporated into ONs), and 2) RNA-skeleton probes (ONs containing pyrenyl residue attached to 2′-*O*-position of adenosine). The pyrene-labeled ONs differ in: 1) the nature of the tether that links pyrene to the nucleotide, 2) the nature of the sugar that carries the pyrene chromophore (altritol or ribose), 3) the nature of the backbone (HNA or RNA), and 4) the number of chromophores on the oligonucleotide. The thermal stability, the absorbance and the fluorescence properties of the probes and complexes were investigated. The HNA- and RNA-pyrene-labeled probes show differences in absorbance and fluorescence properties when hybridized with RNA targets; this reflects the structural differences in the probe–target interaction. Especially the di-chromophoric probes turned out to be efficient to signal hybridization, by virtue of their disappearing aggregate/excimer emission upon hybridization. We use the expression "aggregate/excimer" as excitation spectra reveal that the multichromophoric species show spectral characteristics as well of aggregates as of excimers (see the Supporting Information).

This system represents the first example of a probe to detect the hybridization of oligonucleotides by probing the disappearance of aggregate/excimer emission.[22–24]

Results and Discussion

Design and synthesis of pyrene-labeled probes

Several ONs containing 2′-*O*-(pyren-1-ylmethyl)uridine[25] were prepared and used as fluorescent probes of DNA and RNA in hybridization assays.[3–5,25–26] Here we report on the synthesis of ONs containing pyrenyl residue attached to 2′-*O*-position of adenosine with different linkers. Moreover the adenine derivative of 3-*O*-(pyren-1-ylmethyl)-2-deoxy-D-*altro*-hexitol was also incorporated into hexitol ONs.

The structure of the pyrene-labeled adenine nucleotides and the oligonucleotide sequence of the targets and pyrene-labeled probes are shown below. The probes differ in the number of pyrene fluorophores (one, two or three) attached to HNA and RNA oligonucleotides. In the HNA probes, the pyrene fluorophores are linked to altritol nucleotides at the supplementary hydroxyl group, in analogy to the pyrenylated RNA monomers. Altritol nucleic acid (ANA) is an analogue of oligoribonucleotide containing the standard nucleoside bases, but with a phosphorylated 1,5-anhydroaltritol backbone, which can be hybridized sequence-selectively by RNA and which is often used as antisense agents. Hexitol nucleic acids are oligonucleotide derivatives with a six-membered carbohydrate moiety.[27a,b] (For HNA-skeleton probes HA1-1, HA1-2 and HA1-3, and RNA-skeleton probes RA2-1, RA2-2 and RA2-3, the pyrene moiety is connected to the HNA- or RNA skeleton through a methylene group. For the RNA-skeleton probes RA3-2 and RA4-2, the pyrene moiety is connected to the RNA skeleton through an amide carbonyl group). To study the thermal stability of the binding between the pyrene-labeled probes and RNA targets, HNA reference H0 and RNA reference R0 without pyrene were used as standards to bind RNA targets. Here two RNA targets, HP, which has a hairpin motif, and TAR, were used.

HNA-skeleton probes and reference:

- HA1-1: 6′-CAU ACA$_1$* UUC UAC UUG-4′
- HA1-2: 6′-CAU ACA$_1$* UUC UA$_1$*C UUG-4′
- HA1-3: 6′-CA$_1$*U ACA$_1$* UUC UA$_1$*C UUG-4′
- H0: 6′-CAU ACA UUC UAC UUG-4′

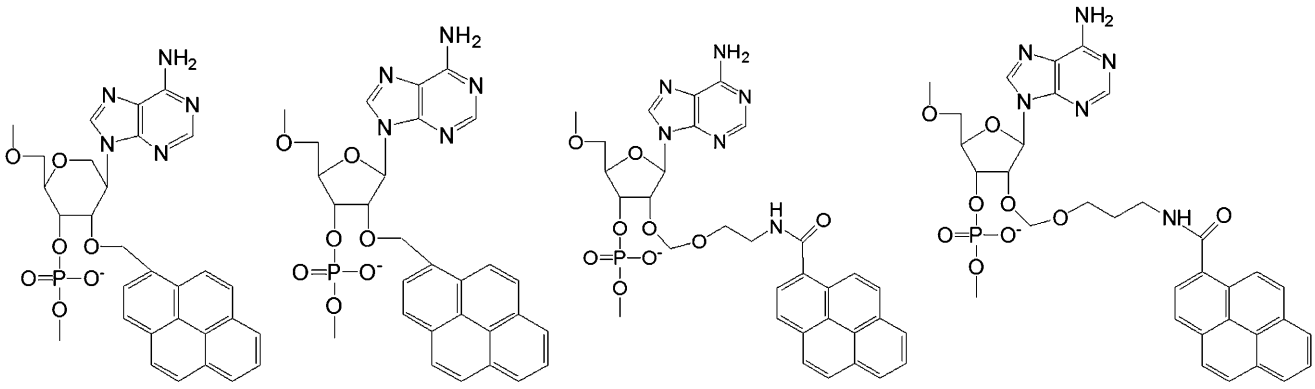

A$_1$* A$_2$* A$_3$* A$_4$*

RNA-skeleton probes and reference:

- RA2-1: 5′-CAU ACA_2* UUC UAC UUG-3′
- RA2-2: 5′-CAU ACA_2* UUC UA_2*C UUG-3′
- RA2-3: 5′-CA_2*U ACA_2* UUC UA_2*C UUG-3′
- RA3-2: 5′-CAU ACA_3* UUC UA_3*C UUG-3′
- RA4-2: 5′-CAU ACA_4* UUC UA_4*C UUG-3′
- R0: 5′-CAU ACA UUC UAC UUG-3′

RNA targets:

- HP: 5′-GCA CAA ACA AGU AGA AUG UAU GUG C-3′
- TAR: 5′-CAA GUA GAA UGU AUG-3′

Synthetic approach for the pyrenylated ANA monomer: Benzoylation of altritol nucleoside **1**[28] using a transient protection procedure[29] gave the 3′-*O*-trimethylsilyl(TMS) derivative **2** instead of the desired nucleoside **2**. The TMS group was found to be stable under standard ammonium hydroxide treatment; its cleavage required the presence of fluoride anion. Condensation of the sodium salt of **2** with pyren-1-ylmethyl chloride in DMF gave its 3′-*O*-pyren-1-ylmethyl derivative (**3**) in 42% yield (Scheme 1). After acidic deblocking, nucleoside **4** was obtained, which was converted into monomethoxytrityl derivative **5** and finally amidite **6.**

Synthetic approach for RNA-skeleton probes RA2-n: 2′-*O*-(Pyren-1-ylmethyl)uridine derivatives were prepared by alkylation of 3′,5′-*O*-bis-trityluridine with pyren-1-ylmethyl chloride in the presence potassium hydroxide in benzene–dioxane mixture under reflux conditions.[25] For the preparation of 2′-*O*-(pyren-1-ylmethyl)adenosine we used the modified alkylation procedure of 9-(5-*O*-trityl-β-D-ribofuranosyl)-N^6-trityladenine (**7**) developed by Pfleiderer et al.[30–31] Condensation of the sodium salt of **7** with pyren-1-ylmethyl chloride in DMF resulted in a mixture containing 2′-*O*-(pyren-1-ylmethyl)adenosine derivative **8** and its 3′-isomer in a 5:1 ratio as main products and some traces of starting nucleoside **7** and **2′,3′-***O*-bis-(pyren-1-ylmethyl) derivative. The desired 2′-isomer **7** was obtained in 48% yield after double crystallization from acetone. The structure of 2′-isomer **8** was proved by COSY spectra, cross peaks between 3′-OH and 3′-H, 3′-H and 2′-H, 2′-H and 1′-H could be observed. After detritylation 2′-*O*-(pyren-1-ylmethyl)adenosine (**9**) was prepared and converted to the required amidite **12** via usual reaction sequence **10**→**11**→**12** in overall good yield (Scheme 2).

Synthetic approach for RNA-skeleton probes RA3-2 and RA4-2: The RA3-2 and RA4-2 probes with pyrene-carboxamide chromophores attached via longer linkers, were prepared according to Scheme 3 by using recently developed methodology.[32–34] Condensation of 3′,5′-*O*-blocked adenosine **13** with excess of **14a,b** in the presence of tin tetrachloride in 1,2-dichloroethane at −12 °C for 40 min gave products **15a,b** in the yields of 54–56%. Selective cleavage of the trifluoroacetyl group was accomplished using 8 M $MeNH_2$ in ethanol and following condensation with *N*-hydroxysuccinimidylpyrene-1-carboxylate in the presence of DBU compounds **16a,b** were obtained (yields 75–78% for two steps). *N*-benzoylation afforded nucleosides **17a,b**, which were converted into desired amidites **20a,b** via the usual reaction sequence **18**→**19**→**20** in overall good yield (Scheme 3).

The structures of the prepared compounds were established by NMR and MS. It should be mentioned that some of the ^{1}H NMR spectra of the obtained compounds, especially altritol derivatives, are rather complicated due to the overlap of signals of the adenosine residue and the diastereotopic protons of CH_2Pyr, OCH_2CH_2O and $CH_2OCH_2CH_2CH_2O$ groups. In spite of this, most of the chemical shifts and coupling constants may be calculated directly from NMR spectra. In some cases double resonance, ^{1}H,^{13}C correlation and COSY spectra were used for the assignment.

Synthesis and purification of oligonucleotides: Oligonucleotide assembly was performed with an Expedite™ DNA synthesizer (Applied Biosystems) by using the phosphoramidite approach (see the Experimental Section).

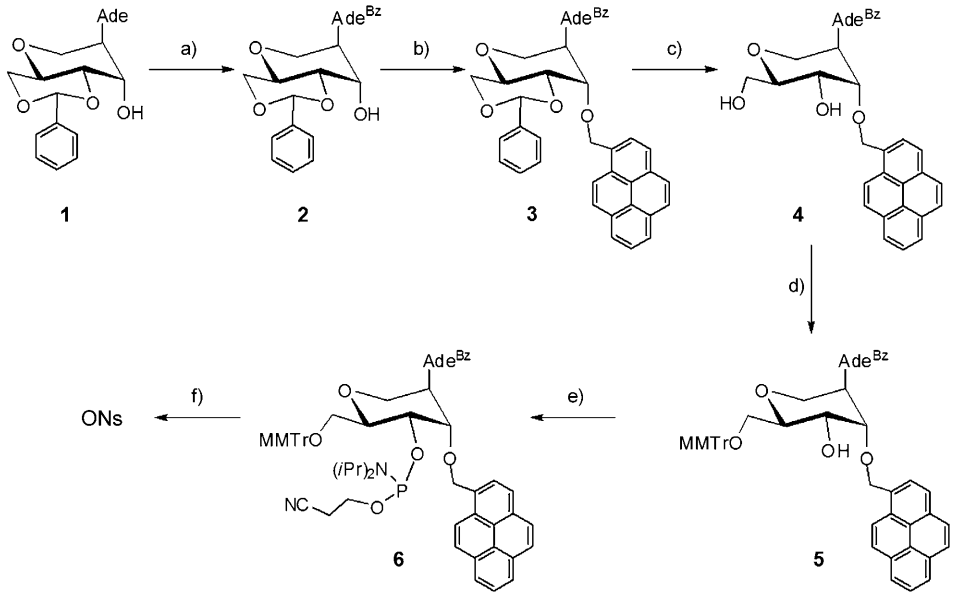

Scheme 1. a) TMSCl/pyridine, 20 °C, 1 h, BzCl/pyridine, 20 °C, 2 h, 4% NH_4OH, NH_4F/pyridine, 20 °C, 1 h (yield 64%); b) 1-(chloromethyl)pyrene, NaH/DMF, −5 °C, 4 h (yield 42%); c) TFA/dichloroethane, 0 °C, 40 min (yield 61%); d) MMTrCl/pyridine, 20 °C, 24 h (yield 74%); e) $iPr_2NPCl(OCH_2CH_2CN)$, iPr_2NEt/dichloromethane, 20 °C, 4 h (yield 61%); f) automated oligonucleotide synthesis. Ade: adenine; Bz: benzoyl; MMTr: monomethoxytrityl.

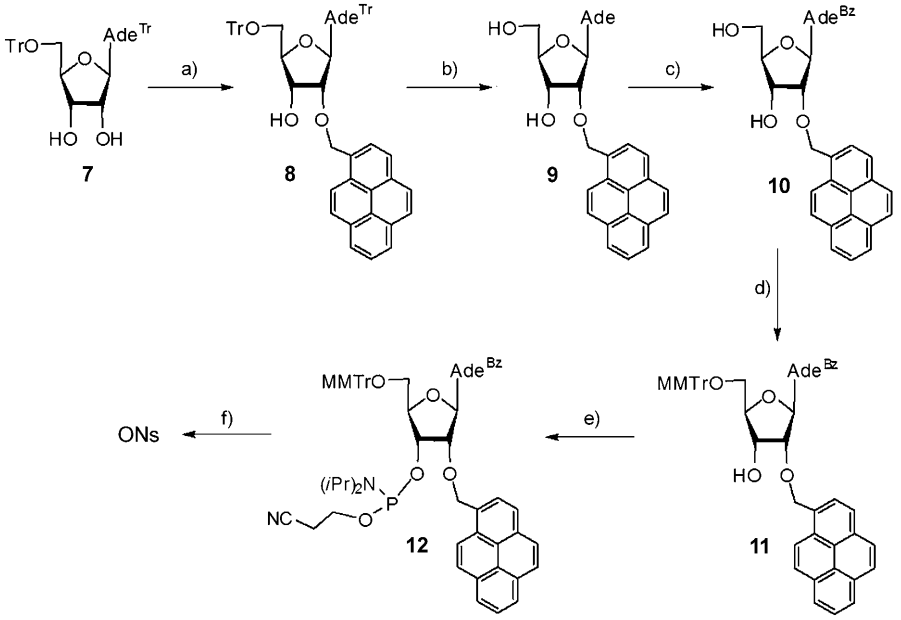

Scheme 2. a) 1-(Chloromethyl)pyrene, NaH/DMF, 0 °C, 30 min (yield 48%); b) 80% AcOH, 120 °C, 30 min (yield 66%); c) TMSCl/pyridine, 20 °C, 1 h, BzCl/pyridine, 20 °C, 2 h, 4% NH_4OH, 20 °C, 1 h (yield 68%); d) MMTrCl/pyridine, 20 °C, 24 h (yield 83%); e) $iPr_2NPCl(OCH_2CH_2CN)$, iPr_2NEt/dichloromethane, 20 °C, 4 h (yield 89%); f) automated oligonucleotide synthesis. Ade: adenine; Bz: benzoyl; Tr: trityl.

RNA hybridization

HNA-skeleton probes (A_1)*

Absorption spectra: As an example, the temperature-dependent absorption spectra of the HNA probe HA1-2 and its complexes are shown in Figure 1. The corresponding spectra of HA1-1 and HA1-3 are documented in the Supporting Information (Figure S2). In all cases, for the probes the pyrene absorption band at 349 nm blue-shifts gradually to 346 nm upon increasing the temperature from 10 to 80 °C (Figure 1A). Yet for the HA1-*n*/TAR mixtures the pyrene absorption band at 343 nm red-shifts to 347 nm upon increasing the temperature (Figure 1B and C). Thus, the spectral shift of pyrene absorption can be used to monitor the hybridization of oligonucleotides: the absorption band of pyrene peaks at 343 nm for the duplexes compared to 349 nm for the single stranded probe.

In contrast to HA1-1, which shows a comparable shift for mixtures with HP, the pyrene absorption band peaks already at 347 nm at room temperature and changes very little with increasing temperature for HA1-2/HP and HA1-3/HP mixtures. This suggests that the multichromophoric probes do not complex efficiently with HP. The formation of a hairpin structure is expected to compete with the hybridization of the probe.

Melting curves: The UV-melting curves monitored at 260 nm for the HNA-skeleton probes (HA1-*n*), the HNA reference (H0), which is a HNA ON, and RNA reference (R0), with TAR and HP are shown in Figure 2 (see also Table 1 for melting points). With increasing number of pyrene units in the HNA-skeleton probes, the melting point decreases: the stability of the duplexes becomes lower the more pyrene chromophores the probes contain. The melting curves with TAR (Figure 2A) show a more clear melting profile than those with HP (Figure 2B): the melting curves with HP reflect the melting of the hairpin structures rather than the interaction with probes or references.

Fluorescence spectra: The fluorescence spectra of HNA-skeleton probes HA1-1 and HA1-2 and "complexes" with RNA targets TAR and HP at 20 °C are shown in Figure 3A and B, respectively. For these probes the emission fine structure of pyrene is lost and there are only two bands in the vicinity of 378 and 398 nm. In addition, HA1-2 and HA1-3 (Figure S5) also show aggregate/excimer emission with a maximum around 480 nm.

It should be noted that this long wavelength emission shows characteristics of excimer as well as of aggregate emission. The excitation spectrum of this emission (see the Supporting Information) clearly indicates a significant increase of the relative intensity of the 0–1 band compared to that of the 0–0 transition while at the same time the 0–0 transition is shifted to the red. On the other hand the long wavelength part of the emission spectrum is completely featureless, strongly broadened and red shifted. It is absolutely not a mirror image of the excitation spectrum. While the first observation points to aggregates, the second one is characteristic for excimers.

The aggregate/excimer emission is attributed to single strand folding. The fluorescence intensities and spectra of the mixtures with TAR and HP differ little from those of single stranded probe HA1-1 (Figure 3A). Yet for the multichromophoric systems (Figure 3B), the fluorescence intensity at 378 nm in presence of TAR or HP is significantly larger than that for the probes themselves: for HA1-2/TAR, the fluorescence intensity is even twice that of HA1-2. In addition, the complexes of the multichromophoric probes with TAR do not show aggregate/excimer emission anymore (Table 1). Only for HA1-2/HP and HA1-3/HP is aggregate/excimer emission still observed. Again, this is attributed to only partial duplex formation with the hairpin structure; this leaves free probe monomer in solution.

Temperature-dependent fluorescence spectra of HNA-skeleton probes and their complexes confirm the interpretation (Figure S5) of the temperature dependent absorption spectra. HA1-1 never shows aggregate/excimer emission at any temperature, while the multichromophoric probes HA1-2 and HA1-3 always show aggregate/excimer emission around 480 nm. Yet for their mixtures with TAR, aggregate/excimer emission is essentially only observed at higher temperatures (HA1-2/TAR:

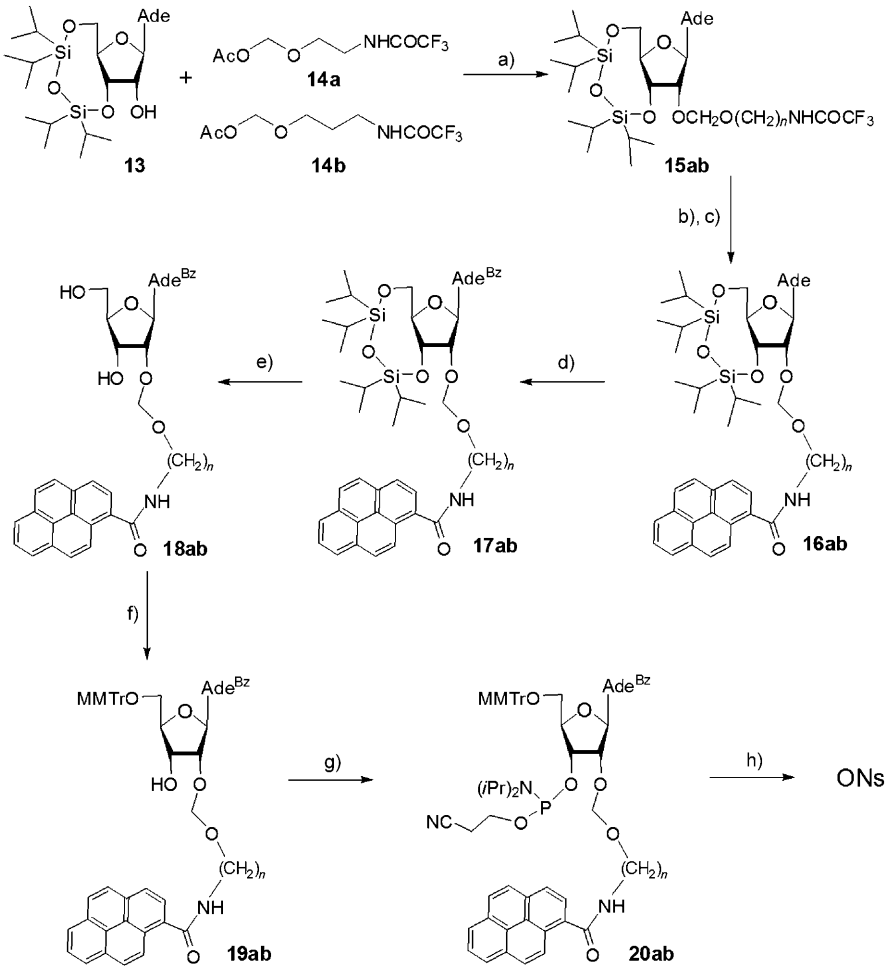

Scheme 3. a) $SnCl_4$/dichloroethane, −12 °C, 40 min (yield 54–56%); b) 8 M $MeNH_2$/ethanol, 35 °C, 6 h; c) *N*-hydroxysuccinimidylpyrene-1-carboxylate, DBU/dichloroethane, 20 °C, 4 h (yield 75–78% for two steps); d) BzCl/pyridine, 20 °C, 2 h, 4% NH_4OH, 20 °C, 1 h (yield 73–77%); e) Bu_4NF/THF, 20 °C, 15 min (yield 85–91%); f) MMTrCl/pyridine, 20 °C, 24 h (yield 76–82%); g) $iPr_2NPCl(OCH_2CH_2CN)$, iPr_2NEt/dichloromethane, 20 °C, 4 h (yield 82% for **20a**; 67% for **20b**); h) automated oligonucleotide synthesis. For compounds **15a**–**20a**, $n=2$, for compounds **15b**–**20b**, $n=3$; Ade: adenine; Bz: benzoyl.

40 °C; HA1-3/TAR: 30 °C). As the appearance of the aggregate/excimer emission is attributed to the denaturation of the complexes, the lower temperature at which aggregate/excimer emission appears for HA1-3/TAR indicates the lower stability of the latter complex. This is in line with the stability trend suggested by the UV/Vis melting curves.

For complexes HA1-2/HP and HA1-3/HP, aggregate/excimer emission appears almost as for the single stranded probes, which is attributed to a considerable fraction of noncomplexed single stranded probes.

Note that the pyrene fluorescence emission intensity is expected to decrease with increasing temperature.[35–36] The emission band at 378 nm is higher than that at 398 nm at low temperature, but this situation is reversed at high temperature. The temperature dependent changes in intensity of these two bands suggest a decrease in polarizability at high temperature. This holds both for the pure HNA-skeleton probes and mixed with targets.

These tendencies could be quantified by monitoring the monomer to aggregate/excimer intensity ratio I_M/I_E[37–38] at different temperatures (Table 1).

RNA-skeleton probes:

2′-O-(1-pyrenylmethyl) tether: A_2*

Absorption spectra: The temperature-dependent absorption spectra of the complexes of RNA-skeleton probes RA2-1, RA2-2 and RA2-3 with TAR are shown in Figure 4. For the RNA-skeleton probes, the absorption band at 351 nm gradually blue-shifts to 347 nm. This indicates a decreased polarizability: the contact with RNA bases is replaced by contact with water upon increasing the temperature from 10 to 80 °C. Yet for the mixtures, the absorption band of pyrene at 351 nm does not shift until denaturation sets in; this induces a blue-shift to 347 nm.

The absorption band of pyrene blue-shifts gradually upon increasing the temperature both for single stranded RNA- (from 351 nm to 347 nm) and HNA-skeleton probes (from 349 nm to 346 nm). Though, it is important to note the different temperature-dependent spectral shift upon denaturation of the complexes: HNA-skeleton probes from 343 nm to 347 nm; RNA-skeleton probes from 351 nm to 347 nm. This suggests that the micro environment of pyrene is different for both types of probes upon complexation. The absorption of polyaromatic intercalators including pyrene is known to shift to longer wavelengths upon π-stacking with nucleobases.[39] In line with these arguments, we suggest that for RNA-skeleton probes, pyrene is intercalated upon hybridization, while for HNA-skeleton probes, the pyrene molecules are relatively free from interaction with the nucleobases.

Melting curves: The UV-melting curves monitored at 260 nm for the RNA-skeleton probes/RNA complexes are shown in Figure 5. The melting point of complexes RA2-1/TAR, RA2-2/TAR, and RA2-3/TAR is 52, 45, and 42 °C, respectively, and decreases again with increasing number of pyrene units in the RNA-skeleton probes (Figure 5). The melting points of complex RA2-1/HP, RA2-2/HP and RA2-3/HP are probe independent (Fig-

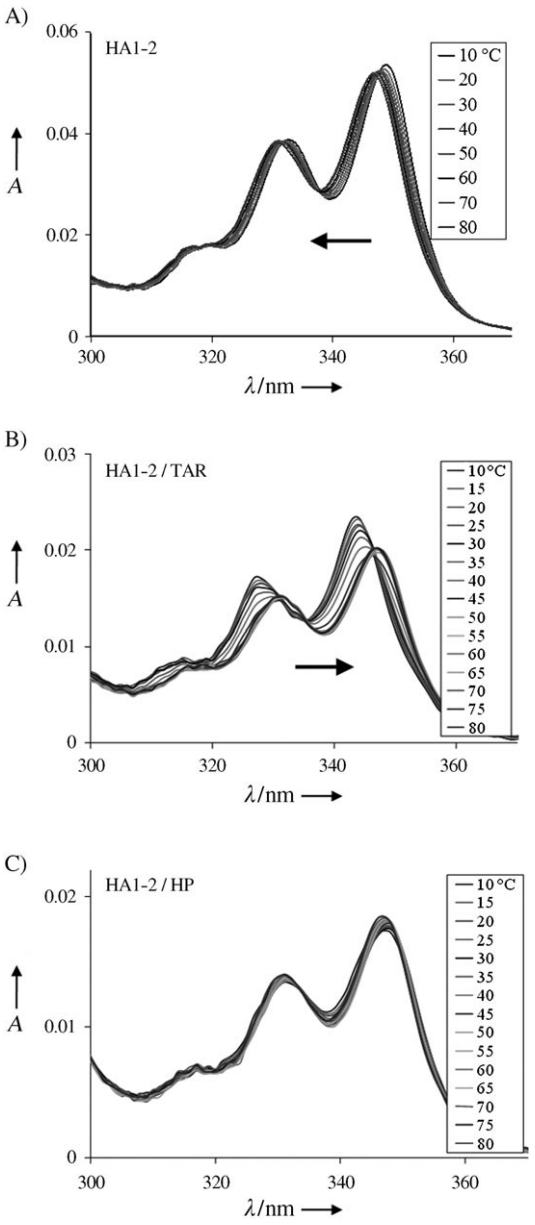

Figure 1. Temperature-dependent absorption spectra of HNA-skeleton probes and their complexes. A) HA1-2 (1 μM); B) HA1-2/TAR (4 μM); C) HA1-2/HP (4 μM); Spectra of the probes and their mixture with TAR and HP were recorded using optical cells with a path length of 1 cm and 1 mm, respectively. The arrow indicates the spectral shift upon increasing the temperature.

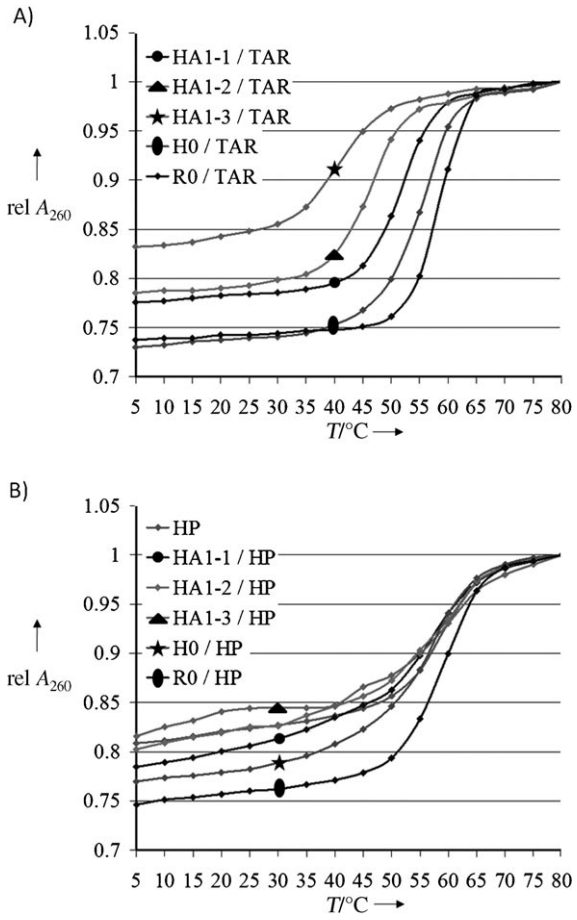

Figure 2. UV-melting curves monitored at 260 nm for: A) HNA-skeleton probes/TAR, H0/TAR and R0/TAR and B) HP, HNA-skeleton probes/HP, H0/HP and R0/HP; concentration is ~4 μM.

ure S8). This is attributed to the hairpin formation of HP (melting point is 57 °C).

Note that the melting points of the complexes with RNA-skeleton probes are higher than those with HNA-skeleton probes by 2–5 °C; this indicates a higher stability of the complexes with the RNA-skeleton probes and is remarkable in view of the increased affinity of HNA and HNA probes which was described before.[27]

Fluorescence spectra: The fluorescence spectra of RNA-skeleton probes RA2-1 and RA2-2 and their complexes with RNA targets TAR and HP at 20 °C are shown in Figure 6. The fluorescence intensity of RA2-1 is affected very little by duplex formation (Figure 6A). Yet Figure 6B shows a great difference in fluorescence profile and intensity between RA2-2 and its mixtures, especially RA2-2/TAR. It is important to note again (see SI) that the excitation spectra of the long wavelength emission differ in the same way from those of the 378 nm emission as observed for HA1-2 and HA1-3. The fluorescence of RA2-2 is dominated by aggregate/excimer emission, peaking at around 490 nm. RA2-2/TAR shows only monomer emission. The fluorescence intensity at 377 nm of RA2-2/TAR is about nine times that of RA2-2. RA2-3 also shows aggregate/excimer emission, but to a smaller extent than RA2-2 (Figure S6). As a result, though the aggregate/excimer emission also disappears for RA2-3/TAR, the overall change/gain in monomer emission is much lower. Mixtures of the probes with the hairpin RNA target HP do not show a similar strong decrease in the aggregate/excimer emission region and enhanced fluorescence in the monomer region. Note that the fluorescence quantum yields (Table 1) are lower than those of HNA-skeleton probes.

Temperature-dependent fluorescence spectra (Figure S6) of the RNA-skeleton probes RA2-1, RA2-2 and RA2-3 mixed with TAR reveal that the fluorescence intensities in the monomer region of the single stranded probes decrease with increasing temperature. Though RA2-2 and RA2-3 show aggregate/

Table 1. Melting temperatures of pyrene-labeled oligonucleotide mixtures, fluorescence quantum yields and monomer/excimer ratios of the pyrene-labeled oligonucleotides and their mixtures.

Single strands or complexes	T_m[a] [°C] (±2)	Φ_f[b] (Φ_M, Φ_E) (±0.002)	I_M/I_E[c] (±0.2)	
			20 °C	70 °C
HA1-1	–	0.055	∞[d]	∞
HA1-1/TAR	50	0.052	∞	∞
HA1-1/HP	50	0.050	∞	∞
HA1-2	**–**	**0.055 (0.041, 0.014)**	**6.5**	**2.8**
HA1-2/TAR	**45**	**0.098**	∞	**2.6**
HA1-2/HP	50	0.084 (0.071, 0.013)	11.4	2.8
HA1-3	–	0.056 (0.040, 0.016)	5.9	1.7
HA1-3/TAR	40	0.075	∞	1.7
HA1-3/HP	50	0.065 (0.052, 0.013)	7.8	1.7
HP	57	N.A.	N.A.	N.A.
RA2-1	–	0.009	∞	∞
RA2-1/TAR	52	0.010	∞	∞
RA2-1/HP	55	0.009	∞	∞
RA2-2	**–**	**0.025 (0.003, 0.022)**	**0.5**	**1.6**
RA2-2/TAR	**45**	**0.019**	∞	**1.6**
RA2-2/HP	55	0.030 (0.012, 0.018)	1.5	1.6
RA2-3	–	0.036 (0.016, 0.019)	1.9	1.6
RA2-3/TAR	42	0.047	∞	1.7
RA2-3/HP	55	0.040 (0.021, 0.019)	2.3	1.7
RA3-2	**–**	**0.22 (0.16, 0.06)**	**6.2**	**2.9**
RA3-2/TAR	**60**	**0.23**	∞[d]	**2.9**
RA3-2/HP	58	0.26	∞	2.9
RA4-2	**–**	**0.20 (0.10, 0.10)**	**2.3**	**1.5**
RA4-2/TAR	**55**	**0.25**	∞	**1.4**
RA4-2/HP	55	0.24	∞	1.5

[a] All samples are aqueous solutions (pH 7.5, 0.1 M NaCl, 20 mM potassium bihydrogen phosphate, 0.1 mM EDTA) without degassing oxygen; melting temperatures were monitored at 260 nm. [b] Quantum yields were measured at 20°; quinine sulfate in 1.0 N sulfuric acid was used as a standard; Φ_M, Φ_E are quantum yields in monomer and aggregate/excimer emission region, respectively. [c] Ratio of emission maxima for monomer (half-sum of the emission intensity at 378 and 398 nm) and aggregate/excimer (intensity at around 480 nm) fluorescence at 20 and 70 °C. [d] ∞ denotes that there is no aggregate/excimer emission.

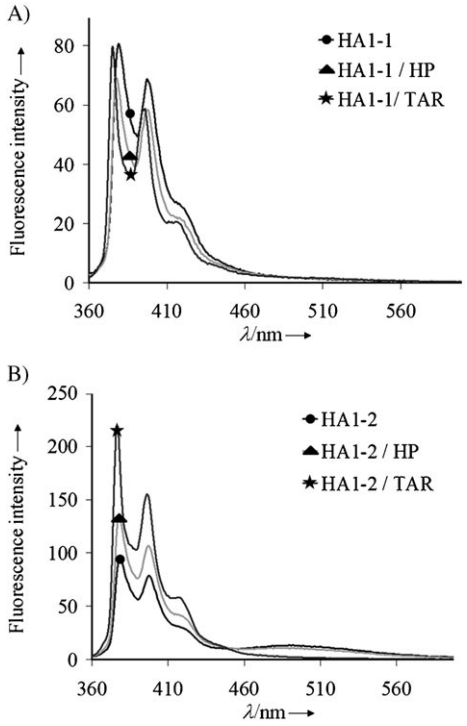

Figure 3. A) Fluorescence spectra of HNA-skeleton probe HA1-1 and the complexes with RNA targets TAR and HP at room temperature. B) Fluorescence spectra of HNA-skeleton probe HA1-2 and its mixture with RNA targets TAR and HP at room temperature. Probe and target concentration was 0.16 μM; the excitation wavelength was 350 nm.

excimer emission, for RA2-2/TAR and RA2-3/TAR no aggregate/excimer emission is observed until denaturation sets in. The monomer to aggregate/excimer intensity ratios I_M/I_E at 20 and 70 °C are listed in Table 1.

Hybridization suppresses aggregate/excimer emission and enhances monomer emission of probes that carry two or three pyrene labels. This effect is most pronounced for RA2-2.

The multichromophoric RA2-*n* probes show, relative to the monomer emission, a more intense aggregate/excimer emission than the multichromophoric HA1-*n* probes. Combined with the larger stability of the RA2-*n*/TAR complexes, RA2-2 is the most promising probe, despite its lower fluorescence quantum yield.

Pyrene-carboxamide tether: A_3 and A_4**

The drawback of the 2′-*O*-(1-pyrenylmethyl) probe is the low fluorescence quantum yield. Therefore, we also explored a pyrene-carboxamide chromophore because of its known larger fluorescence quantum yield. The fluorescence spectra and quantum yields of pyrene-carboxaldehyde are known to be highly dependent on the solvent polarity too.[6,40] It has been used as a base-discriminating fluorescent DNA probe to detect the microenvironment of DNA duplexes and sense the difference in polarities between the inside and the outside of the duplexes.[6] Here we attached a pyrene-carboxamide chromophore to the RNA skeleton, and thus prepared probes RA3-2 and RA4-2.

Absorption spectra: The temperature-dependent absorption spectra of RA3-2 with the targets are shown in Figure 7 (For RA4-2, Figure S4). For the probes the absorption maximum of pyrene blue-shifts gradually from 349 to 345 nm with increasing temperature. The complexes with the RNA-skeleton probe with the methylene tether (for example, RA2-2/TAR) show a blue-shift only upon denaturation; for RA3-2/TAR, the pyrene peak blue-shifts upon denaturation from 353 nm to 344 nm; for the other mixtures, the pyrene peak blue-shifts from 351 to 344 nm.

Melting curves: The UV-melting curves are shown in Figure 8. The melting points of RA3-2/TAR (60 °C) and RA4-2/TAR (55 °C) are considerably higher than for RA2-*n*/TAR (45 °C). The amide carbonyl tethers lead to more stable complexes. The melting points of RA3-2/HP and RA4-2/HP are 58 and 55 °C, respectively; these are comparable to the melting point of HP. However, in contrast to the RNA-skeleton probes with a methylene linker, there is evidence for hybridization with HP based upon

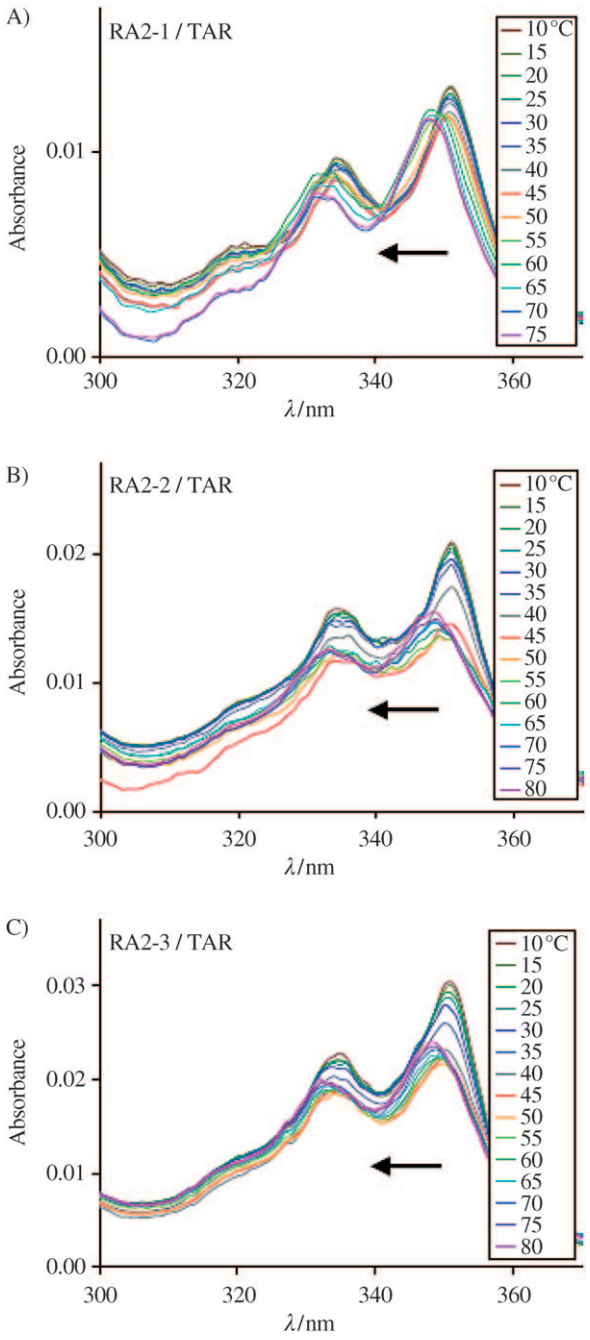

Figure 4. Temperature-dependent absorption spectra of RNA-skeleton probes and their complexes with TAR. A) RA2-1/TAR; B) complex RA2-2/TAR; C) complex RA2-3/TAR. Spectra were recorded at 4 μM in optical cells with a 1 mm path length. The arrow indicates the spectral shift upon increasing the temperature.

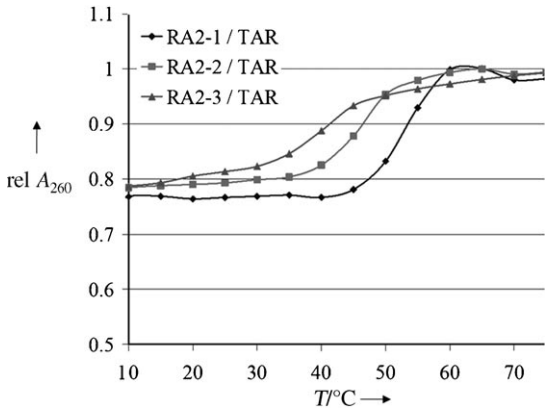

Figure 5. UV-melting curves monitored at 260 nm for RNA-skeleton probes/TAR. Concentration was ~4 μM.

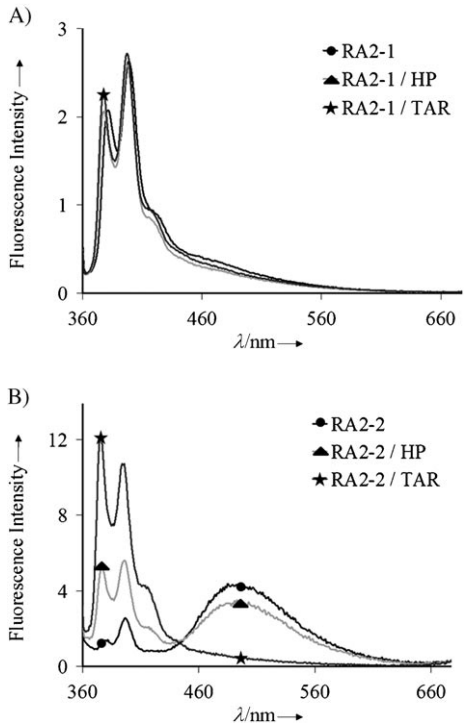

Figure 6. A) Fluorescence spectra of RNA-skeleton probe RA2-1 and the complexes with RNA targets TAR and HP at room temperature. B) Fluorescence spectra of RNA-skeleton probe RA2-2 and the complexes with RNA targets TAR and HP at room temperature. Spectra were recorded at 0.16 μM at 20 °C upon excitation at 350 nm.

temperature dependent fluorescence measurements (Figure S7).

Fluorescence spectra: The fluorescence spectra of RNA-skeleton probes RA3-2 and RA4-2 and their complexes with RNA targets TAR and HP at 20 °C are shown in Figure 9. Only one band appears in the monomer emission, yet there are two bands in the vicinity of 378 and 398 nm for HNA- and RNA-skeleton probes with methylene tethers. In this case, the fine structure of pyrene monomer emission is lost completely as was also observed in DNA probes with pyrene-carboxamide chromophores.[6] Like the other probes with two or three pyrene units, both RA3-2 and RA4-2 show aggregate/excimer emission. When compared to those of emission below 420 nm the main maximum of the excitation spectra of the long wavelength emission is broadened towards longer wavelengths. Furthermore a shoulder is observed around 380 nm. This behavior is analogous to that observed for HA1-2, HA1-3, RA2-2 and RA2-3. Note that RA4-2 shows a stronger aggregate/excimer emission than RA3-2. A longer linker favors the increased aggregate/excimer emission. The aggregate/excimer emission

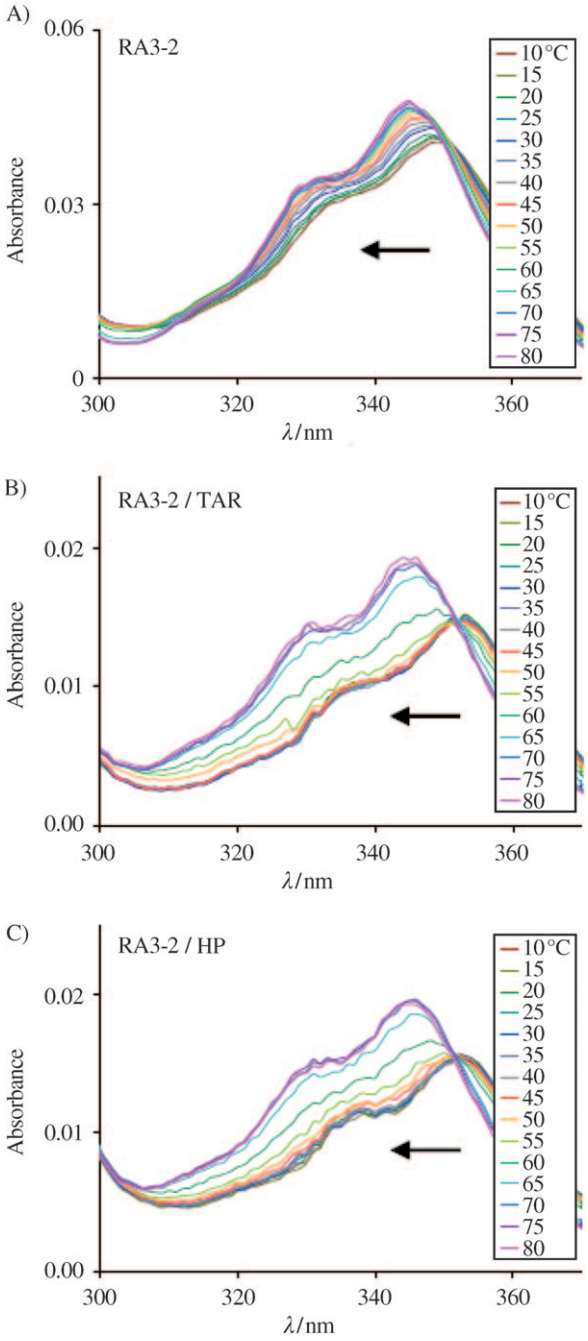

Figure 7. Temperature-dependent absorption spectra of RNA-skeleton probes with pyrene-carboxaldehyde chromophores and their complexes between 300 and 370 nm. A) RA3-2; B) RA3-2/TAR; C) RA3-2/HP; spectra of the probes and their mixture with TAR and HP were recorded by using optical cells with a path length of 1 cm and 1 mm, respectively. The arrow indicates the spectral shift upon increasing the temperature.

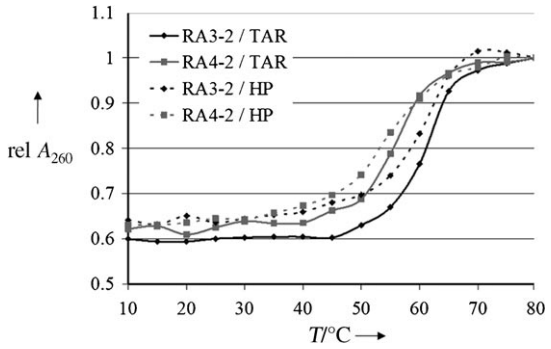

Figure 8. UV-melting curves monitored at 260 nm for mixtures of pyrene-carboxamide labeled RNA-skeleton probes and targets; concentration was ~4 μM.

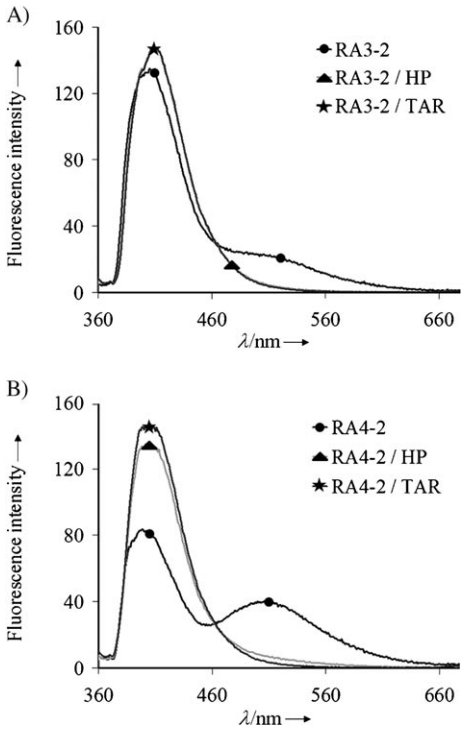

Figure 9. A) Fluorescence spectra of RNA-skeleton probe RA3-2 and the complexes with RNA targets TAR and HP. B) Fluorescence spectra of RNA-skeleton probe RA4-2 and the complexes with RNA targets TAR and HP. Spectra were recorded at 0.16 μM at 20 °C upon excitation at 350 nm.

disappears upon hybridization. In case of RA3-2, the monomer fluorescence intensity is only weakly enhanced upon duplex formation (Figure 9A), while for RA4-2, the monomer emission intensity is almost doubled (Figure 9B). The quantum yields of the probes in single stranded form and double stranded form are shown in Table 1. All the probes with amide carbonyl tethers show higher fluorescence quantum yields than those with methylene tethers. For example, the quantum yield of RA3-2 is 0.22 and that of RA2-2 is only 0.025.

Temperature-dependent fluorescence spectra of RA3-2 and RA4-2 (Figure S7 in the Supporting Information) and their mixtures with targets show that the fluorescence intensities in the monomer emission region decrease with increasing temperature. The probes show aggregate/excimer emission over the complete temperature range yet upon addition of the target, aggregate/excimer emission is only observed for denatured systems. The monomer to aggregate/excimer intensity ratio I_M/I_E at 20 °C and 70 °C is listed in Table 1.

In contrast with RA1-*n* and RA2-*n*, mixtures with hairpin HP exhibit only little aggregate/excimer emission below 20 °C; this indicates that the pyrene-carboxamide probes hybridize with the hairpin target effectively. The amide carbonyl tethers lead to more stable complexes, and this is consistent with the conclusion drawn from the melting curves.

Conclusions

We have explored two kinds of pyrene-labeled probes (HNA- and RNA-skeleton probes) to detect RNA hybridization. The effect of probe skeleton (HNA or RNA), the number of pyrene fluorophores (one, two or three), and the nature of the tether linking pyrene to the skeleton on the thermal stability, absorption and fluorescence properties of the complexes was investigated and compared with the properties of the single stranded probes.

The melting curves show that complexes of RNA-skeleton probes are more stable than those of HNA-skeleton probes. Also the nature of the linker connecting the pyrene chromophores to the skeleton plays a role: complexes of RNA-skeleton probes with pyrene-carboxamide groups are more stable than those of RNA-skeleton probes attached by pyrene-methylene groups.

With an increasing number of pyrene units in the probes, the melting point and therefore the stability of the duplexes decrease.

As far as the fluorescence characteristics are concerned, significant changes are only observed upon hybridization for the multichromophoric probes. Namely, the aggregate/excimer emission of the free probes disappears upon hybridization and simultaneously, the monomer emission intensity increases. In general, the probes carrying two pyrene units perform better than those with three pyrene units, as far as the changes in fluorescence intensity are concerned upon hybridization. Two probes outperform clearly the others for TAR recognition: RA2-2 and RA4-2. In absolute numbers, the relative intensity change (monomer vs. aggregate/excimer emission) is more pronounced for RA2-2/TAR than for RA4-2. Note though that the quantum yield of fluorescence is about 10 times larger for RA4-2 than for RA2-2.

Most of the probes interact well with TAR but not with the hairpin HP, except for the RNA-skeleton probes with pyrene-carboxamide amide groups, for which the aggregate/excimer emission disappears upon mixing RA3-2 or RA4-2 with HP.

To detect the hybridization of ONs by probing the disappearance of aggregate/excimer emission might turn out to be useful in biological fluorescence assays.

Experimental Section

Sample solutions: Samples were prepared under buffered conditions (20 mM KH_2PO_4, 0.1 M NaCl, 0.1 mM EDTA, pH 7.5 adjusted by NaOH). Complexes were prepared from a 1:1 mixture of ONs (4 μM). The mixed solution was heated at 80 °C for 5 min and then cooled to room temperature over 30 minutes. Samples were not degassed prior to the fluorescence experiments.

UV/Vis absorption: Measurements were carried out by using a Perkin–Elmer UV/Vis spectrometer Lambda 40. Temperature-dependant absorbance measurements for the complexes were carried out using a 1 mm path length cell; other measurements were carried out using a 1 cm path length cell.

Steady-state fluorescence: Spectra were recorded by using a Fluorolog FI3-22 fluorometer (Edison, USA) equipped with two double monochromators and correction of the fluorescence spectra for wavelength dependence of the sensitivity of the instrument. Fluorescence quantum yields, Φ, of the pure probes and complexes were determined at 20° by using quinine sulfate in sulfuric acid (1.0 N) as a standard with a known Φ of 0.546. The fluorescence quantum yields were calculated according to the following equation (1)[2]:

$$\Phi_X = \Phi_{ST}[D_X/D_{ST}][A_{ST}/A_X][n_X/n_{ST}] \quad (1)$$

Here, Φ_X and Φ_{ST} are the fluorescence quantum yield of the test and the standard, respectively. D_X and D_{ST} are the area under the fluorescence spectra of the sample and the reference, respectively. A_X and A_{ST} are the respective absorbencies of the sample and reference solution at the wavelength of excitation. n_X and n_{ST} are the values of refractive index for the respective solvents used for the sample and reference. The monomer to aggregate/excimer intensity ratio (I_M/I_E) was calculated by taking the ratio of the half-sum of the emission intensity at 378 and 398 nm to the intensity at around 480 nm.

Acknowledgement

Financial support from the KULeuven research fund (GOA 2/01, IDO/02/014), the Federal Science Policy of Belgium (grant IAP-V-03 and IAP-6/27), from the Institute for the Promotion of Innovation by Science and Technology in Flanders (IWT), and Russian Academy of Sciences (Program "Molecular and Cell Biology") is acknowledged. We thank C. Jackers for recording the excitation spectra.

Keywords: fluorescence · HNA · hybridization · pyrene · RNA

[1] Y. Tor (ed.), *Tetrahedron* **2007**, *63*, Issue 17.
[2] F. M. Winnik, *Chem. Rev.* **1993**, *93*, 587–614.
[3] M. Nakamura, Y. Fukunaga, K. Sasa, Y. Ohtoshi, K. Kanaori, H. Hayashi, H. Nakano, K. Yamana, *Nucleic Acids Res.* **2005**, *33*, 5887–5895.
[4] K. Yamana, H. Zako, K. Asazuma, R. Iwase, H. Nakano, A. Murakami, *Angew. Chem.* **2001**, *113*, 1138–1140; *Angew. Chem. Int. Ed.* **2001**, *40*, 1104–1106.
[5] K. Yamana, R. Iwase, S. Furutani, H. Tsuchida, H. Zako, T. Yamaoka, A. Murakami, *Nucleic Acids Res.* **1999**, *27*, 2387–2392.
[6] A. Okamoto, K. Kanatani, I. Saito, *J. Am. Chem. Soc.* **2004**, *126*, 4820–4827.
[7] J. Telser, K. A. Cruickshank, L. E. Morrison, T. L. Netzel, *J. Am. Chem. Soc.* **1989**, *111*, 6966–6976.
[8] M. K. Smalley, S. K. Silverman, *Nucleic Acids Res.* **2006**, *34*, 152–164.
[9] J. N. Wilson, Y. Cho, S. Tan, A. Cuppoletti, E. T. Kool, *ChemBioChem* **2008**, *9*, 279–285.
[10] T. L. Netzel, M. Zhao, K. Nafisi, J. Headrich, M. S. Sigman, B. E. Eaton, *J. Am. Chem. Soc.* **1995**, *117*, 9119–9128.
[11] M. Manoharan, K. L. Tivel, M. Zhao, K. Nafisi, T. L. Netzel, *J. Phys. Chem.* **1995**, *99*, 17461–17472.
[12] K. Nakatani, S. Saito, I. Saito, *Nat. Biotechnol.* **2001**, *19*, 51–55.
[13] A. Okamoto, K. Tainaka, I. Saito, *J. Am. Chem. Soc.* **2003**, *125*, 4972–4973.

[14] P. Conlon, C. Y. J. Yang, Y. R. Wu, Y. Chen, K. Martinez, Y. Kim, N. Stevens, A. A. Marti, S. Jockusch, N. J. Turro, W. H. Tan, *J. Am. Chem. Soc.* **2008**, *130*, 336–342.
[15] E. Mayer-Enthart, H. A. Wagenknecht, *Angew. Chem.* **2006**, *118*, 3451–3453; *Angew. Chem. Int. Ed.* **2006**, *45*, 3372–3375.
[16] V. L. Malinovskii, F. Samain, R. Häner, *Angew. Chem.* **2007**, *119*, 4548–4551; *Angew. Chem. Int. Ed.* **2007**, *46*, 4464–4467.
[17] K. Yamana, Y. Fukunaga, Y. Ohtani, S. Sato, M. Nakamura, W. J. Kim, T. Akaike, A. Maruyama, *Chem. Commun.* **2005**, 2509–2511.
[18] K. Yamana, T. Iwai, Y. Ohtani, S. Sato, M. Nakamura, H. Nakano, *Bioconjugate Chem.* **2002**, *13*, 1266–1273.
[19] A. Mahara, R. Iwase, T. Sakamoto, K. Yamana, T. Yamaoka, A. Murakami, *Angew. Chem.* **2002**, *114*, 3800–3802; *Angew. Chem. Int. Ed.* **2002**, *41*, 3648–3650.
[20] A. Okamoto, T. Ichiba, I. Saito, *J. Am. Chem. Soc.* **2004**, *126*, 8364–8365.
[21] F. D. Lewis, Y. Zhan, R. L. Letsinger, *J. Am. Chem. Soc.* **1997**, *119*, 5451–5452.
[22] R. T. Ranasinghe, T. Brown, *Chem. Commun.* **2005**, 5487–5502.
[23] C. A. Royer, *Chem. Rev.* **2006**, *106*, 1769–1784.
[24] A. P. Silverman, E. T. Kool, *Chem. Rev.* **2006**, *106*, 3775–3789.
[25] K. Yamana, Y. Ohashi, K. Nunota, M. Kitamura, H. Nakano, O. Sangen, T. Shimidzu, *Tetrahedron Lett.* **1991**, *32*, 6347–6350.
[26] M. Nakamura, Y. Ohtoshi, K. Yamana, *Chem. Commun.* **2005**, 5163–5165.
[27] a) B. Allart, K. Khan, H. Rosemeyer, G. Schepers, C. Hendrix, K. Rothenbacher, F. Seela, A. Van Aerschot, P. Herdewijn, *Chem. Eur. J.* **1999**, *5*, 2424–2431; b) C. Hendrix, H. Rosemeyer, I. Verheggen, F. Seela, A. Van Aerschot, P. Herdewijn, *Chem. Eur. J.* **1997**, *3*, 110–120.
[28] B. Allart, R. Busson, J. Rozenski, A. Van Aerschot, P. Herdewijn, *Tetrahedron* **1999**, *55*, 6527–6546.
[29] G. S. Ti, B. L. Gaffney, R. A. Jones, *J. Am. Chem. Soc.* **1982**, *104*, 1316–1319.
[30] H. U. Blank, D. Frahne, A. Myles, W. Pfleiderer, *Liebigs Ann. Chem.* **1970**, *742*, 34–42.
[31] A. Myles, W. Pfleiderer, *Chem. Ber.* **1972**, *105*, 3327–3333.
[32] G. V. Bobkov, K. V. Brilliantov, S. N. Mikhailov, J. Rozenski, A. Van Aerschot, P. Herdewijn, *Chem. Commun.* **2006**, *71*, 804–819.
[33] S. N. Mikhailov, G. V. Bobkov, K. V. Brilliantov, J. Rozenski, A. Van Aerschot, P. Herdewijn, M. H. Fisher, R. L. Juliano, *Nucleosides Nucleotides Nucleic Acids* **2007**, *26*, 1509–1512.
[34] E. V. Efimtseva, I. V. Kulikova, S. N. Mikhailov, *Curr. Org. Chem.* **2007**, *11*, 337–354.
[35] C. Honda, Y. Katsumata, R. Yasutome, S. Yamazaki, S. Ishii, K. Matsuoka, K. Endo, *J. Photochem. Photobiol. A* **2006**, *182*, 151–157.
[36] G. Vicq, A. M. Bottreau, J. M. Fornies-Marquina, *J. Mol. Liq.* **1988**, *38*, 233–265.
[37] D. F. Anghel, V. Alderson, F. M. Winnik, M. Mizusaki, Y. Morishima, *Polymer* **1998**, *39*, 3035–3044.
[38] B. Haldar, A. Mallick, N. Chattopadhyay, *J. Photochem. Photobiol. B* **2005**, *80*, 217–224.
[39] N. Cho, S. A. Asher, *J. Am. Chem. Soc.* **1993**, *115*, 6349–6356.
[40] A. P. De Silva, H. Q. N. Gunaratne, T. Gunnlauson, A. J. M. Huxley, C. P. McCoy, J. T. Rademacher, T. E. Rice, *Chem. Rev.* **1997**, *97*, 1515–1566.
[41] A. Van Aerschot, T. Saison-Behmoaras, J. Rozenski, C. Hendrix, G. Schepers, G. Verhoeven, P. Herdewijn, *Bull. Soc. Chim. Belges* **1995**, *104*, 717–720.

Received: January 21, 2009
Published online on April 16, 2009

